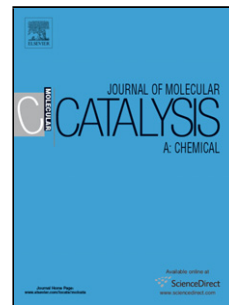# Accepted Manuscript

Title: n-Octanol oxidation on Au/TiO$_2$ catalysts promoted with La and Ce oxides

Author: Y. Kotolevich E. Kolobova E. Khramov M.H. Farías Ya. Zubavichus H. Tiznado S. Martínez-González V. Cortés Corberán J.D. Mota-Morales A. Pestryakov N. Bogdanchikova

Please cite this article as: Y.Kotolevich, E.Kolobova, E.Khramov, M.H.Farías, Ya.Zubavichus, H.Tiznado, S.Martínez-González, V.Cortés Corberán, J.D.Mota-Morales, A.Pestryakov, N.Bogdanchikova, n-Octanol oxidation on Au/TiO2 catalysts promoted with La and Ce oxides, Journal of Molecular Catalysis A: Chemical http://dx.doi.org/10.1016/j.molcata.2016.09.003

n-Octanol oxidation on Au/TiO$_2$ catalysts promoted with La and Ce oxides

Y. Kotolevich[a], E. Kolobova[b], E. Khramov[c], M.H. Farías[a], Ya. Zubavichus[c], H. Tiznado[a], S. Martínez-González[e], V. Cortés Corberán[e], J. D. Mota-Morales[a,f], A. Pestryakov[b], N. Bogdanchikova[a]

[a] Centro de Nanociencias y Nanotecnología (CNyN), Universidad Nacional Autónoma de México (UNAM), Ensenada, 22860, México

[b] Tomsk Polytechnic University, Tomsk, 634050 Russia

[c] National Research Center "Kurchatov Institute", Moscow, 123182 Russia

[d] Centro de Investigación Científica y de Educación superior de Ensenada, Ensenada, 22860, México

[e] Institute of Catalysis and Petroleumchemistry (ICP), CSIC, 28049 Madrid

[f] CONACYT - Centro de Nanociencias y Nanotecnología (CNyN), Universidad Nacional Autónoma de México (UNAM), Ensenada, 22860, México

Graphical abstract
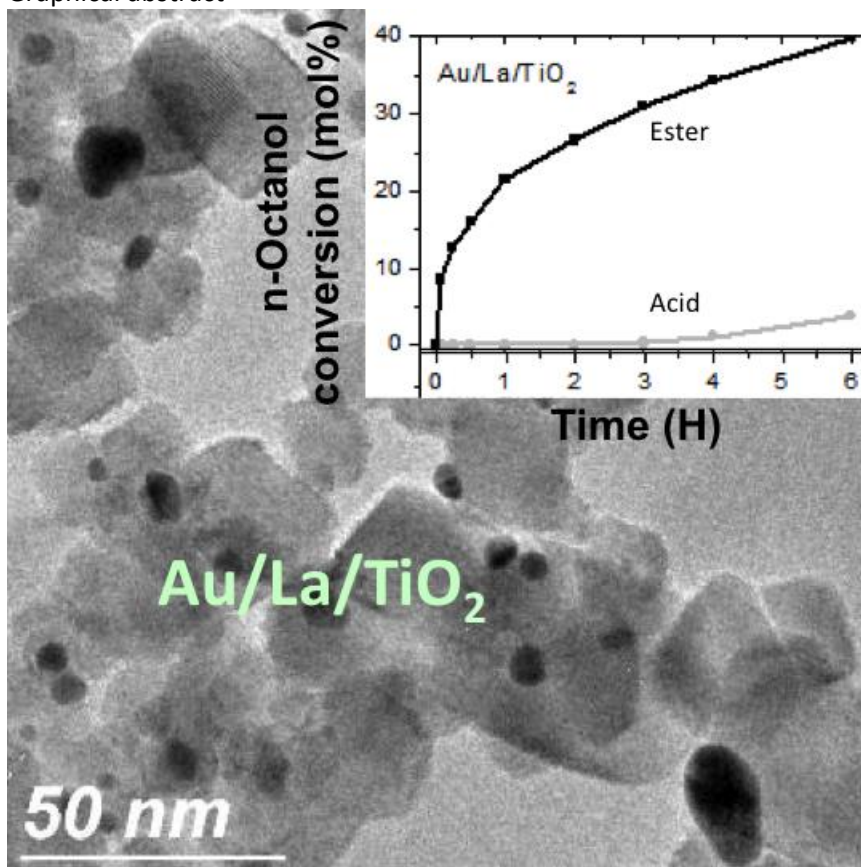
Highlights

- Nanogold supported on TiO$_2$ proved effective in catalytic base-free oxidation of n-octanol in liquid phase under mild conditions of temperature and pressure.
- La and Ce oxides acted as promoters, where La$_2$O$_3$-modified catalyst enhanced the oxidation of n-octanol to four-fold as compared with unmodified catalyst.
- Au/La/TiO$_2$ give rise to the highest ester selectivity at isoconversion with no acid formation.
- Au^{3+} ions were excluded as gold active sites in n-octanol oxidation while intermediate oxidation states promoted by La and Ce are more likely involved

Abstract

This study aims to improve gold-based catalyst effectiveness in *n*-octanol oxidation by adjusting the structural and electronic properties of gold through incorporation of additives to support. Au/La/TiO$_2$, Au/Ce/TiO$_2$, and Au/TiO$_2$ catalysts, prepared by deposition-precipitation with urea, were tested in the base-free oxidation of octanol under mild conditions in liquid phase. The influence of additives on structural properties of the catalyst and the active phase, and on the electronic and redox properties of the active gold species was studied by TEM, SR-XRD, EXAFS, FTIR of adsorbed CO, and XPS. Support modifiers affected gold particle size distribution, but no direct dependence of the catalyst activity on Au NPs average size was observed. The activity of as-prepared catalysts was limited, and even lower in the presence of modifiers at that stage. Reductive pretreatment boosted the activity of every catalyst, and support modification with La and Ce increased four- and two-fold, respectively, the activity of Au/TiO$_2$ under the same reaction conditions. The nature of modifiers also affected the product distribution where the outstanding performance of Au/La/TiO$_2$ gives rise to the highest ester selectivity at isoconversion with no acid formation. Overall, the studied catalysts, and especially Au/Ce/TiO$_2$, and Au/La/TiO$_2$, hold promise for *n*-octanol oxidation under mild conditions.

Introduction

Industrial oxidation processes are usually based on the use of stoichiometric oxidizing agents and/or alkalis; these conditions are considered as environmentally unfriendly. This drives the need to develop catalytic processes to obtain organic compounds using oxidants such as air or molecular oxygen at atmospheric pressure. Gold-containing catalysts are of great interest for industrial and environmentally sustainable reactions [1]. They have received a great deal of attention due to the high catalytic activity that gold nanoparticles (Au NPs) deposited have shown in several oxidation processes. Their major advantage, compared with other catalysts, relies on their ability to carry out liquid-phase oxidation under mild conditions, including atmospheric pressure and relatively low temperatures (below 140°C) [2]. Despite the unique catalytic properties of nanogold catalysts, a number of issues remain unsolved [3-5]. Among others, their fast deactivation, either during working or storage, represents a serious problem for their practical implementation [6-14]. Understanding on the mechanisms underlying the

deactivation of gold and the way it can be solved will greatly advance the development of the theory and practice of synthesis of active catalysts based on gold nanoparticles.

Nanosized gold-based catalysts are among the most investigated systems for aerobic green oxidation of all types of alcohols in liquid phase [15]. *n*-Octanol is often used for comparative studies of catalyst activity in oxidation of alcohols as a convenient model of primary alcohols of long chain, also called fatty alcohols. Thus, a number of gold catalysts have been tested for 1-octanol oxidation over the last years. Because this oxidation is more difficult than that of most alcohols of industrial importance, it is expected that catalysts active for n-octanol oxidation will be also efficient in similar processes for other similar molecules resulting from biomass transformations. The use of bases during alcohol oxidation requires the neutralization of carboxylates formed with strong acids, which generates large amount of waste in the form of inorganic salts of variable pH. This justifies the need of catalyzing oxidation of alcohols to acid and esters in the absence of bases, i.e. by green processes.

Though n-octanol is frequently used for comparative purposes there are very few studies specifically devoted to its liquid-phase oxidation on gold catalysts under the mild conditions in the recent literature [15]. Prati's group first reported the base-free oxidation of 1-octanol with O_2 over Au NPs supported on nanometer-sized NiO [16]. Haruta's group [17] reported an extensive and specific study of base-free oxidation of 1-octanol (in water) over Au NPs with moderate pressure of O_2. Screening of Au NPs supported on a variety of metal oxides (Al_2O_3, TiO_2, MnO_2, Fe_2O_3, Co_3O_4, NiO, ZnO, ZrO_2 and CeO_2) evidenced that their activity and the resulting product distribution depend strongly on the nature of the support and the solvent. All these results were obtained under moderate pressure of oxygen (5 bar). Recently, it has been found that 1-octanol can be oxidized with flowing oxygen at normal pressure and in the absence of a base, using heptane as solvent [18]. The most active gold catalyst for oxidation of octanol under mild conditions found in this screening was $Au/CeO_2/Al_2O_3$ [18, 19]. Since it is known that Al_2O_3 is not an optimal support for gold, the presence of CeO_2 becomes crucial to favor the activity of the catalyst.

Most studies have focused on finding a composition and method of synthesis of catalysts that lead to increase their effectiveness. One strategy has been the use of a second metal additive, like Cu or Pd [20, 21], but monometallic catalysts have demonstrated higher activity than bimetallic ones. However, as catalytic performance of Au NPs depends strongly on the nature of support, we use an alternative strategy based on the modification of the support surface to improve its catalytic performance. So, our group investigated the modification of hexagonal mesoporous silica (HMS) with metal cations having redox properties (Ce, Fe), to use them as supports of gold NPs for aerobic oxidation of n-octanol [22]. It was concluded that support additives modify the redox behavior of supported gold, and the most active catalysts were those in which small charged gold clusters dominated over the other species, e.g. ions, metallic particles, etc. More recently we applied this strategy to titania supports using Fe and Mg oxides as modifiers [23]. It was found that additive with electron-donor properties (MgO) provides the maximum catalytic activity (TON), while electron-acceptor one (Fe oxides) results less effective.

In the present work, we significantly advanced our latter approach by investigating Au/TiO_2 based catalysts modified with two prospective additives, namely oxides of cerium and lanthanum, aiming to improve their performance in the selective oxidation of n-octanol under mild conditions. These modifiers were selected because CeO_2 has proven to be a promoter for Au NPs in n-octanol oxidation [19], whereas Au NPs supported on La_2O_3/TiO_2 show high stability for CO oxidation after long-term storage [24]. The final aim of this work is to shed light on the

nature of gold active sites responsible of the catalytic activity of nanometric gold, which is an unexplored topic for base-free catalytic oxidation of n-octanol.

Results and discussion

Fig. 1 shows the results of catalytic tests of $Au/La/TiO_2$, $Au/Ce/TiO_2$ and Au/TiO_2 catalysts in *n*-octanol oxidation under mild conditions. It can be observed that activity of as-prepared samples was very low (Fig. 1a); actually the reaction started after 1, 2 and 3 h for Au/TiO_2, $Au/Ce/TiO_2$ and $Au/La/TiO_2$, respectively, reaching ≤ 5% conversion after 6 h in all cases.

Addition of modifiers had little and even deleterious effect on activity at this stage. Hence, it can be inferred that Au^{3+} (the main state of gold at this stage) is not active because all as-prepared catalysts were not active during the initial period of run time (1-3 h). During the course of the reaction, however, catalyst became slightly active, probably due to partial reduction of gold ions. As expected, after pretreatment in hydrogen, activity increased significantly for all catalysts from the very start of reaction, and both modified samples become much more active than Au/TiO_2, e.g. two-fold for $Au/Ce/TiO_2$ and four-fold for $Au/La/TiO_2$ after 6 hours of run time.

In all tests the main products were octanal and ester, octyl octanoate, while traces of octanoic acid formation were detected only for Au/TiO_2 at longer run times. The type of modifier used also influenced the product distribution (Fig. 1b). With increasing run time, selectivity towards octanyl octanoate increased at the expense of octanal formation. It should be noted that ester appears to be not only secondary product but also primary one (initial selectivity 15-20%).

Baiker's group proposed that formation of ester in the oxidation of octanol on supported Pd catalysts [25] proceeds by oxidation of the initially formed octanal, via hydration to a germinal diol, to the acid, which in turn is esterified with the starting alcohol (Scheme 1, route A). Besides this route, Ishida et al. [17] in their study of n-octanol oxidation on Au catalysts, proposed one alternative route; octanol dehydrogenation gives octanal (as in the route A) that reacts with a second alcohol molecule to form the hemiacetal, which in turn can be oxidized to octyl octanate (Scheme 1, route B). The latter seems the most likely scenario in this case, given than ester is a primary product during the first minutes of the reaction.

It is important to note that octanol activation, and hence octanal formation, occurs only on the gold surface. Formation of octanoic acid and octyl octanoate occurs through intermediates formed by acid-base catalyzed reactions. Two stages are then drawn: the first, octanal formation on gold, and the second, formation of acid and ester due to acid-base reactions occurring mainly on the support surface. In this second stage, water traces and Bronsted and Lewis acid character of supports become more relevant. Differences in ester formation along reaction time were observed among the catalysts, which could be interpreted as due to different acid/base character of their surface. Hence, when and in what extent acid/base stages are involved in the catalytic process may determine the selectivity towards acid or ester.

Several factor have to be taken into account to understand the change of catalytic properties as result of catalysts promotion; changes on structural properties of catalyst (specific surface, porous structure, content of active phase), changes on structural properties of the active phase (average size, size distribution, crystallinity of the Au NPs) and variation of electronic and redox properties of the active component are just a few. To clarify this, several catalysts properties were investigated as described below.

Table 1 summarizes the catalysts' specific surface area (S_{BET}) and Au content. S_{BET} of the TiO_2 support was reduced (around 20%) after modification with all modifiers. Nevertheless, S_{BET} of modified supports and all the catalysts were identical; this ruled out this parameter as the source of their distinct catalytic performance. The Au content is similar for modified catalysts, though somewhat higher for Au/TiO_2.

.

Fig. 2 presents the results of TGA performed on all catalysts. Thermograms of the supports (not shown) differed little among them, and they displayed peaks in the range of 40-50°C corresponding to the loss of adsorbed water. At higher temperatures a double-peaked curve corresponding to the removal of the first (152-165°C) and the second (201-209°C) amino groups of urea used as a precipitating agent for gold ions appeared [26]. No weight loss was observed above 250°C, which indicates that pretreatment at 300 °C guarantees a complete decomposition of the organic precursors.

Particle size distribution of gold catalysts, calculated from HRTEM images, is displayed in Fig. 3. The most monodispersed distribution was observed on Au/TiO_2 with an average diameter of 3.7 nm (Fig. 3 a). The histogram for $Au/La/TiO_2$ (Fig. 3 b) was slightly narrower (1-7 nm), with an average size (2.8 nm) lower than that of Au/TiO_2. The Au particle sizes range of $Au/Ce/TiO_2$ (Fig. 3 c) was broader (1-13 nm) and shifted to larger sizes compared with the other samples, with an average particle size of 4.7 nm. The average particle size in the investigated catalytic systems decreases in the following order: $Au/Ce/TiO_2$ > Au/TiO_2 > $Au/La/TiO_2$. Thus, direct correlation between Au NPs average size and their performance for catalytic activity could not be established. However, one should take into account that for numerous reactions not all metal particles visible on the micrographs are active participants in the catalytic process; for some cases, only particles with size of 1 nm and less are active as reported in the literature and in our previous work [27-34].

SR-XRD diffraction patterns of gold catalysts after hydrogen pretreatment show that the phase composition of the support (rutile/anatase) is not significantly altered (Fig. 4). Bragg peaks of the gold phase are more intense for Au/TiO_2 than for the modified support catalysts. It can be due to the higher Au content in this catalyst (Table 1). CeO_2 phase (average crystal size ca.~10 nm) is also revealed in $Au/Ce/TiO_2$, which may indicate that cerium oxide was not homogeneously distributed on the surface of TiO_2 but it rather concentrated into nanoparticles, as reported earlier by our group [22, 43].

Structural parameters of Au particles obtained from Rietveld refinement of SR-XRD patterns are presented in Table 2. The lattice parameter of gold decreased in the order Au/TiO_2 > $Au/Ce/TiO_2$ > $Au/La/TiO_2$, which is a consequence of the efficient gold dispersion in the latter than in the former catalyst [35-39]. This sequence correlates well with the trend of catalytic activity of studied samples, but contradicts that of particle size distributions obtained by TEM. Stokes microstrains of gold particles (Table 2), indicative of the concentration of defects (vacancies and dislocations at the interfaces between crystallites) [40-42] decreased in the order: $Au/Ce/TiO_2$>$Au/La/TiO_2$>Au/TiO_2. In cases of $Au/Ce/TiO_2$ and $Au/La/TiO_2$ the size measured by TEM (Fig. 3) and SR-XRD (Table 2) are in good agreement: 4.7 and 4.7 nm for $Au/Ce/TiO_2$ and 2.8 and 5.1 nm for $Au/La/TiO_2$, respectively. In Au/TiO_2, the average particle size of Au estimated from Bragg peak broadening (17.7 nm) is much larger than the value obtained

from TEM data (3.7 nm). This suggests that in TEM data about Au particles with size ~ 17.7 nm were not taken into account because of they relatively low abundance.

In Fig. 5 Au L_3 edge EXAFS data for the reduced catalysts are shown. The peak at R≈2.5 Å corresponds to the first coordination sphere in Au metal structure. The decrease in the intensity of this peak suggests that the first coordination number of Au is decreased in the order: Au/TiO_2 > $Au/Ce/TiO_2$ > $Au/La/TiO_2$ (see Tab. 4). This indicates that Au particles formed on the modified supports are smaller than on pure TiO_2, which apparently contradicts the TEM particle size distribution for $Au/Ce/TiO_2$ but is consistent with SR-XRD results [44-46]. According to TEM data the broadest particle distribution and the largest particles of nano-Au were observed for $Au/Ce/TiO_2$. This is due to the fact described above: in $Au/Ce/TiO_2$ the modifier was not dispersed homogeneously. For all catalysts Au L_3-edge XANES spectra shape are similar to the spectrum of Au foil, indicating the presence of Au only in reduced state Au^0 and the absence of oxidized Au species.

As it can be seen in Fig. 6, intense peaks of absorption (200-400 nm) in the DRS spectra of supports were observed in the region typical for the charge transfer transitions of Au^+ and Au^{3+} with ligands, or for absorption bands due to the transition of electrons between molecular orbitals of few-atomic clusters, e.g. $Au_n^{\delta+}$, n<10. [47-54]. This makes difficult applying this method for the investigation of these Au species. After hydrogen treatment catalyst samples exhibited bands in the region 550-570 nm, which correspond to plasmon resonance of metallic Au NPs [47, 55-59]. As no significant differences were observed in the visible range of the spectra of all samples, it can be concluded that the observed differences in catalytic activity after H_2 pretreatments cannot be caused by metallic Au particles.

Two methods of characterization were gold surface are described Below. CO adsorption at room temperature can be used to identify gold species (e.g. $Au_n^{\delta-}$, Au^0, $Au_n^{\delta+}$, Au^+ [52]). This method was applied to find a correlation between these adsorbed CO species and gold catalytic activity in n-octanol oxidation. Fig. 7 shows the FTIR spectra of adsorbed CO on studied catalysts. Regardless the pretreatment conditions, an intense absorption band at 2102 - 2105 cm^{-1}, attributed to the surface carbonyls of gold atoms Au^0-CO, was observed for all studied samples [60]. Interestingly, the intensity and wavenumber of the band remained irrespective of the redox pretreatment.
Another absorption band at 2143 - 2145 cm^{-1}, related to the complexes Au^+-CO, was observed only in $Au/Ce/TiO_2$ and $Au/La/TiO_2$, i.e., in the catalysts with modified support. An absorption shoulder at 2120 cm^{-1}, attributed to the carbonyls of reduced gold, was observed for Au/TiO_2; however, its relatively high v_{CO} wavenumber indicates that these gold states are electron deficient ($Au_n^{\delta+}$), probably due to the influence of support. It is important to point out that the presence of gold in Au^{3+} state cannot be detected by FTIR CO since it does not adsorb CO under the studied conditions [61]. Au^0-CO peaks were very similar in shape and intensity for all catalysts, despite of their large differences in activity; thus, it can be concluded that the differences in activity are not directly linked to the presence of Au^0 species.

Au^+-CO peak was clearly stronger for $Au/La/TiO_2$ (followed by $Au/Ce/TiO_2$). As indicated above, about half of the particles have 1-2 nm in size for this sample, denoting a higher metal-support interaction. Smaller particle size means higher metal surface area that in principle could explain the higher catalytic activity. If that would be the case, $Au/Ce/TiO_2$ should show the

lowest activity. A better explanation for the observed differences in activity is given if it is considered that both support modifiers, Ce and La, play an active role in the reaction by promoting the formation of Au^+ sites - in the case of La with the added benefit of stabilizing smaller Au particle sizes - improving the catalytic activity as seen in our results.

In order to get deeper insights, the activity assigned to the unit of gold surface, turnover number (TON), was calculated for each catalyst (Fig. 8), and compared to the reported TON of a set of related catalysts $Au/Mg/TiO_2$ and $Au/Fe/TiO_2$ from our recent work [23].

The lowest values of TON were observed for Au/TiO_2, while the highest ones corresponded to $Au/Ce/TiO_2$ and $Au/La/TiO_2$; compared to them, $Au/Mg/TiO_2$ and $Au/Fe/TiO_2$ presented intermediate values (Fig. 8). Initial TON (after the first 5 min) for $Au/Ce/TiO_2$ (0.8) and $Au/La/TiO_2$ (0.6) are roughly 4- and 3-fold higher, respectively, than that for Au/TiO_2 (0.21). Initial TON for $Au/Mg/TiO_2$ (0.4) took intermediate position. These differences decreased along the time (Fig. 8): only ~33% after 6 h, while it was ~400% after 5 min. If Au^+ site, detected by CO adsorbed at room temperature, is an active site, then $Au/La/TiO_2$ should show higher TON than $Au/Ce/TiO_2$. Thus, Au^+ sites cannot be responsible for the activity of studied catalysts in n-octanol oxidation under mild conditions assayed here.

XPS was used for a more detailed study of changes of gold electronic state under the influence of support. Fig. 9 presents the XPS spectra of Au 4f lines of the catalysts after H_2 pretreatment in order of decreasing TON. Both Au $4f_{7/2}$ and $4f_{5/2}$ peaks for all samples required deconvolution, because their widths exceeded those corresponding to a single state. The binding energy (BE) and relative atomic concentration of the various gold species identified in accordance with literature assignments [62-69] are given in Table 3.

The band that corresponds to Au^0 (BE = 84.1 eV) was observed only for low active catalysts, namely $Au/Mg/TiO_2$, $Au/Fe/TiO_2$ and Au/TiO_2. In all samples most of gold surface (68-81%) showed BE in the range of 83.3-83.5 eV, attributed to $Au_n^{\delta-}$ states. The shift to lower BE (as compared to metallic gold) observed in supported gold clusters or nanoparticles can be attributed to several effects. One could be an electron transfer from the support to the gold nanoparticles, accompanied by negative charging of the particles [70-72]. Another plausible scenarios are an increased gold-support interaction with local structural changes, support phase transition of oxide [73, 74] or new compound formation [75]. Finally, a critical factor in determining the negative BE shift of supported gold nanoparticles could be particle shapes, as spherical particles have less coordinated surface atoms, which reduces their BE relative to nanoparticles with large faces [76].

Bands corresponding to cation state Au^+ were registered for $Au/La/TiO_2$, $Au/Ce/TiO_2$, $Au/Fe/TiO_2$ and Au/TiO_2 with relative atomic concentration contributions of 19, 18 and 9%, respectively. A band at BE = 85.7 eV was registered in $Au/Ce/TiO_2$, $Au/Mg/TiO_2$ and $Au/Fe/TiO_2$, which corresponds to gold oxides Au_xO_y [77].

Additives with strong electron-donor (MgO) and strong electron-acceptor (Fe_xO_y) properties resulted ineffective as they modified the electronic state of gold to highly reduced states and highly oxidized states, respectively; affecting the catalytic activity of $Au/Fe/TiO_2$ and $Au/Mg/TiO_2$. On the other hand, additives with moderate electron-donor (La_2O_3) and moderate electron-acceptor (CeO_2) properties lead to a reasonable oxidation of gold surface as compared to Au/TiO_2. It can be concluded that $Au/La/TiO_2$ and $Au/Ce/TiO_2$ promote an optimal gold electron stage content that provides high catalytic activity in *n*-octanol oxidation under mild conditions.

Experimental

Catalysts preparation

Titania Degussa P25 (45 m^2 g^{-1}, nonporous, 70% anatase and 30% rutile, purity >99.5%) was used as starting support. Before use, TiO_2 was dried in air at 100°C for at least 24 h. Modification of titania with molar ratio Ti/M (M = La or Ce) = 40 was made by impregnation (2.5 cm^3/g) of initial TiO_2 with aqueous solutions of modifier precursors $Ce(NO_3)_3 \bullet 6H_2O$ or $La(NO_3)_3 \bullet 6H_2O$ from Aldrich. Then, impregnation products were dried at room temperature for 48 h and at 110°C for 4 h, and calcined at 550°C for 4 h. Commercial $HAuCl_4 \bullet 3H_2O$ (Aldrich) was used as gold precursor. Au/TiO_2 and $Au/M/TiO_2$ catalysts (nominal loading 4 wt. % Au) were prepared by deposition–precipitation with urea in the absence of light, following the procedure previously reported [78-80].

Samples characterization

Thermogravimetric analysis (TGA) and differential thermal analysis (DTA) were performed using a TA Instruments SDT-Q600. Sample was heated from ambient temperature up to 500°C at 5°C /min in the nitrogen with a controlled gas flow of 100 mL/min in both TGA and DTA tests. Mass change (wt. %), rate of mass change (wt. %/min), and heat flow were analyzed. Derivative mass changes are plotted as a function of temperature.

Catalyst samples, either as-prepared or pretreated in hydrogen at 300°C for 1 h, were studied by diffuse reflectance UV–visible spectroscopy (DRS) with a CARY 300 SCAN (Varian) spectrophotometer. Optical spectra of Au/TiO_2 or $Au/M/TiO_2$ samples presented in this work were obtained by subtracting the spectra of pure supports from those of catalyst samples.

Fourier transformed infrared spectra (FTIR) of CO adsorbed on the catalysts were recorded by using a Bruker Tensor 27 FTIR spectrometer in transmittance mode with 4 cm^{-1} resolution. *In situ* experiments were carried out in a quartz cell with NaCl windows capable of working at temperatures from -100 to 300°C and pressures from 10^{-2} to 760 Torr. The sample powder was pressed into disks of 13 mm diameter and weight ~ 20 mg. The sample was pretreated in H_2 or O_2 (100 Torr) at 300°C for 1 h and then cooled down to room temperature. After that, H_2 or O_2 was evacuated and CO adsorption (Matheson Research grade, P^0 = 30 Torr) were carried out. CO spectra presented in this work were obtained by subtracting the CO gas phase spectrum.

The samples were pretreated in hydrogen at 300°C for 1 h for studies with all methods described below in "Samples characterization" paragraph.

Textural properties of samples were determined from nitrogen adsorption-desorption isotherms (−196°C) recorded with a Micromeritics TriStar 3000 apparatus. Prior to experiments, samples were degassed at 300°C in vacuum for 5 h. The N2 adsorbed volume was normalized to a standard temperature and pressure. Specific areas of the samples were calculated by applying the BET method to the nitrogen adsorption data within the P/P0 range 0.05–0.25.

A JEOL-5300 scanning electronic microscope (SEM) was utilized for a general sample morphology observation. Gold contents were measured by energy dispersive spectroscopy (EDS) in the same system equipped with a Kevex Superdry detector.

Transmission electronic microscopy (TEM) studies were carried out using a JEM 2100F microscope operating with a 200 kV accelerating voltage. Samples were ground into a fine powder and dispersed ultrasonically in hexane at room temperature. Then, a drop of the suspension was put on a lacey carbon-coated Cu grid. At least ten representative images were taken for each sample. Particle size distribution was obtained by counting ca. 100 particles for each sample.

X-ray powder diffraction was conducted by the step-scanning procedure (step size 0.02°; 0.5 s) with a Philips XPert PRO diffractometer, using Ni-filtered CuKα (λ = 0.15406 nm) radiation. Assignment of crystalline phases was based on the ICDD- 2013 powder diffraction database.

Synchrotron radiation X-ray diffraction (SR-XRD) experiments were carried out as described in [81]. Diffraction patterns of powdered materials were taken in transmission mode at λ = 0.68886 Å, using Fujifilm Imaging Plate 2D detector (exposure time 30 min). The size of Au-containing particles was estimated from diffraction peaks broadening using the Selyakov–Scherrer formula and Fityk software [82]: each diffraction peak was approximated by the pseudo-Voight function with coefficient η either fitted or equal to 0.5. In some cases, full Rietveld analysis [83] was carried out in terms of Jana2006 program [84].

Au L_3 edge EXAFS spectra were taken in transmission mode as described in [81]. The processing of EXAFS spectra was carried out in terms of IFEFFIT software package [85, 86]. EXAFS Fourier transforms were analyzed for k = 2.0–11.6 Å^{-1} with the weight coefficient k^3 and fitted in the range R = 2.0 – 3.2 Å using the phases and amplitudes of photoelectrons scattering calculated in terms of FEFF8 software [87].

The samples were investigated by X-ray photoelectron spectroscopy (XPS) with a SPECS GmbH custom made system using a PHOIBOS 150 WAL hemispherical analyzer and a non-monochromated X-Ray source. All the data were acquired using Al Kα radiation (1486.6 eV, 200 W). A pass-energy of 50 eV, a step size of 0.1 eV/step and a high-intensity lens mode were selected. The diameter of the analyzed area was 3 mm. Charging shifts were referenced against adventitious carbon (C 1s at 284.5 eV). The pressure in the analysis chamber was maintained lower than 1 x 10^{-8} mbar. Catalysts were mounted on a sample holder and kept overnight in high vacuum in the preparation chamber before they were transferred to the analysis chamber of the spectrometer. Energy regions were selected after a general survey and scanned with several sweeps until a good signal-to-noise ratio was observed. The accuracy of the binding energy (BE) values was ±0.1 eV. Spectra are presented without smoothing or background subtraction, with intensity in counts-per-second (CPS). Peak intensities were estimated by calculating the integral of each peak after subtracting a Shirley type background and fitting the experimental peak to a combination of Lorentzian/Gaussian lines with a 30/70 proportion, considering the spin-orbit 4f$_{7/2}$ and 4f$_{5/2}$ doublet with a 4:3 intensity ratio and the same width on all lines.

Catalytic tests

Catalytic measurements of *n*-octanol oxidation were performed with samples either as-prepared or after being treated in pure hydrogen flow at 300°C for 1 h or in pure oxygen flow for 1 h. Typically, supported gold catalyst (substrate/metal (R) = 100 mol/mol) sample was added to 20 mL of *n*-octanol solution (0.1 M) in *n*-heptane as solvent, in four-necked round bottom flask equipped with reflux condenser, oxygen feed, thermometer and a septum cap. The reaction mixture was stirred in a semibatch reactor operated under atmospheric conditions at 80 ºC. Oxygen (30 mL/min) was bubbled through the suspension and reaction was followed for 6 h. Small aliquots of the reacting mixture were obtained during and at the end of the test, by using nylon syringe filters (pore 0.45 μm), for monitoring the reaction progress. Reactants and products were analyzed in a Varian 450 gas chromatograph, using a capillary DB wax column (15 m x 0.548 mm) and He as the carrier gas.

Conclusions

The catalytic performance of gold catalysts supported on titania for the selective oxidation of alcohols under mild conditions can be substantially improved by modifying the support surface with the appropriate modifiers. For instance, by selecting the proper support additive (La and Ce oxides) activity can be increased fourfold, as it was validated in this work for La oxide.

Modification of gold catalysts with Ce and La oxides significantly influences their catalytic properties in n-octanol oxidation, namely by increasing n-octanol conversion and modifying the products selectivity. This improvement is caused by the combined effect of changes in several properties of the deposited metal, mainly its dispersion, its electronic state and distribution among the various electronic states. Based upon the characterization of catalyst it was not possible to identify the active sites responsible for their catalytic activity; however Au^{3+} ions are excluded as candidate for active sites in n-octanol oxidation on $Au/Ce/TiO_2$ and $Au/La/TiO_2$. It is suggested that the proper balance of intermediate oxidation states in the gold surface is responsible for the higher activity exhibited by $Au/La/TiO_2$ towards n-octanol oxidation.

Ongoing research seeks to identify these active species and the implementation of this strategy to new catalytic systems and gold-catalyzed reactions.

Acknowledgements

References

1. P. Kaminski and M. Ziolek, *Applied Catalysis B: Environmental*, 2016, **187**, 328.
2. M. Haruta, *Gold Bulletin*, 2004, **37**, 27.
3. A. N. Pestryakov, V. V. Lunin, N. Bogdanchikova, O. N. Temkin and E. Smolentseva, *Fuel*, 2013, **110**, 48.
4. N. Bogdanchikova, A. Pestryakov, I. Tuzovskaya, T. A. Zepeda, M. H. Farias, H. Tiznado and O. Martynyuk, *Fuel*, 2013, **110**, 40.
5. N. Bogdanchikova, A. Pestryakov, M. H. Farias, J. A. Diaz, M. Avalos and J. Navarrete, *Solid State Sciences*, 2008, **10**, 908.
6. T. Akita, P. Lu, S. Ichikawa, K. Tanaka and M. Haruta, *Surface and Interface Analysis*, 2001, **31**, 73.
7. B. Schumacher, V. Plzak, M. Kinne and R. J. Behm, *Catalysis Letters*, 2003, **89**, 109.
8. F. Moreau and G. C. Bond, *Applied Catalysis A: General*, 2006, **302**, 110.
9. M. Daté, Y. Ichihashi, T. Yamashita, A. Chiorino, F. Boccuzzi and M. Haruta, *Catalysis Today*, 2002, **72**, 89.
10. W.-S. Lee, B.-Z. Wan, C.-N. Kuo, W.-C. Lee and S. Cheng, *Catalysis Communications*, 2007, 8, 1604.

11. M. Haruta, S. Tsubota, T. Kobayashi, H. Kageyama, M. J. Genet and B. Delmon, *Journal of Catalysis*, 1993, **144**, 175.
12. R. Zanella and C. Louis, *Catalysis Today*, 2005, **107**, 768.
13. M. JIA, X. LI, Zhaorigetu, Y. SHEN and Y. LI, *Journal of Rare Earths*, 2011, **29**, 213.
14. Y. Wu, K.-Q. Sun, J. Yu, B.-Q. Xu, G. C. Bond, D. T. Thompson and C. Louis, *Physical Chemistry Chemical Physics*, 2008, **10**, 6399.
15. V. C. Corberán, M. E. González-Pérez, S. Martínez-González and A. Gómez-Avilés, *Applied Catalysis A: General*, 2014, **474**, 211.
16. A. Villa, C. E. Chan-Thaw, G. M. Veith, K. L. More, D. Ferri and L. Prati, *ChemCatChem*, 2011, **3**, 1612.
17. T. Ishida, Y. Ogihara, H. Ohashi, T. Akita, T. Honma, H. Oji and M. Haruta, *ChemSusChem*, 2012, **5**, 2243.
18. A. Gomez-Aviles, S. Martinez-Gonzalez, S. Ivanova, M.I. Dominguez, J.A. Odriozola, R. Fernandez-Lafuente and V. Cortes Corberan, *7th World Congress on Oxidation Catalysis*, June 9-12, 2013, Saint Luis, USA, 93.
19. V. C. Corberán, A. Gómez-Avilés, S. Martínez-González, S. Ivanova, M. I. Domínguez and M. E. González-Pérez, *Catalysis Today*, 2014, **238**, 49.
20. I.-D. Huang, L.M. Polinski, K.K. Rao, US Patent № 4 154 762, 1979.
21. Y. He, J. Feng, G. L. Brett, Y. Liu, P. J. Miedziak, J. K. Edwards and G. J. Hutchings, *ChemSusChem*, 2015, **8**, 3314.
22. S. Martínez-González, A. Gómez-Avilés, O. Martynyuk, A. Pestryakov, N. Bogdanchikova and V. C. Corberán, *Catalysis Today*, 2014, **227**, 65.
23. Y. Kotolevich, E. Kolobova, G. Mamontov, E. Khramov, J. E. Cabrera Ortega, H. Tiznado, and A. Pestryakov, *Catalysis Today*, 2016. doi:10.1016/j.cattod.2016.05.002 - *in press*
24. E. Kolobova, Y. Kotolevich, E. Pakrieva, G. Mamontov, M. Farías, N. Bogdanchikova and A. Pestryakov, *Molecules*, 2016, **21**, 486.
25. R. Zanella, S. Giorgio, C. R. Henry and C. Louis, *The Journal of Physical Chemistry B*, 2002, **106**, 7634.
26. R. Zanella, L. Delannoy and C. Louis, *Applied Catalysis A: General*, 2005, **291**, 62.
27. R. Zanella and C. Louis, *Catalysis Today*, 2005, **107**, 768.
28. A. A. Chernyshov, A. A. Veligzhanin and Y. V. Zubavichus, *Nuclear Instruments and Methods in Physics Research Section A: Accelerators, Spectrometers, Detectors and Associated Equipment*, 2009, **603**, 95.
29. M. Wojdyr, Fityk 0.8.1: A curve fitting and data analysis program, 2007, http://www.unipress.waw.pl/fityk/.
30. H. M. Rietveld, *Journal of Applied Crystallography*, 1969, **2**, 65.
31. Petricek, V., Dusek, M., & Palatinus, L. (2006). JANA2006. The crystallographic computing system.
32. R.B. Athena, A. Hephaestus, *Journal of Synchrotron Radiation*, 2005, **12**, 537.
33. M. Newville, *Journal of Synchrotron Radiation,* 2001, **8**, 322.
34. A. L. Ankudinov, B. Ravel, J. J. Rehr and S. D. Conradson, *Physical Review B*, 1998, **58**, 7565.
35. G. Jenzer, M. S. Schneider, R. Wandeler, T. Mallat and A. Baiker, *Journal of Catalysis*, 2001, **199**, 141.
36. J. P. CHEN and K. ISA, *Journal of the Mass Spectrometry Society of Japan*, 1998, **46**, 299.
37. M. Flytzani-Stephanopoulos and B. C. Gates, *Annual Review of Chemical and Biomolecular Engineering*, 2012, **3**, 545.

38. L. F. Allard, M. Flytzani-Stephanopoulos and S. H. Overbury, *Microscopy and Microanalysis*, 2010, **16**, 375.
39. J. D. Lessard, I. Valsamakis, M. Flytzani-Stephanopoulos, M. Haruta, T. Kobayashi, H. Sano, and G. Martra, *Chemical Communications*, 2012, **48**, 4857.
40. Y. Lee, G. He, A. J. Akey, R. Si, M. Flytzani-Stephanopoulos and I. P. Herman, *Journal of the American Chemical Society*, 2011, **133**, 12952.
41. M. Flytzani-Stephanopoulos, *Accounts of Chemical Research*, 2014, **47**, 783.
42. M. Yang, S. Li, Y. Wang, J. A. Herron, Y. Xu, L. F. Allard and G. J. Hutchings, *Science,* 2014, **346**, 1498.
43. N. Bogdanchikova, A. Pestryakov, J. Navarrete Balañoz, M. Avalos Borja, J. A. Diaz, M. Farias, *Proceedings of Biannual Conference on Chemistry CHEM. 02*, Cairo, Egipt, March 4-7, 2002, 403.
44. N. Bogdanchikova, A. Pestryakov, M. H. Farias, J. A. Diaz, M. Avalos and J. Navarrete, *Solid State Sciences*, 2008, **10**, 908.
45. J. S. Vermaak, C. W. Mays and D. Kuhlmann-Wilsdorf, *Surface Science*, 1968, **12**, 128.
46. C. W. Mays, J. S. Vermaak and D. Kuhlmann-Wilsdorf, *Surface Science*, 1968, **12**, 134.
47. R. Lamber, S. Wetjen, G. Schulz-Ekloff and A. Baalmann, *The Journal of Physical Chemistry*, 1995, **99**, 13834.
48. C. Solliard and M. Flueli, *Surface Science*, 1985, **156**, 487.
49. K. K. Nanda, A. Maisels and F. E. Kruis, *The Journal of Physical Chemistry C*, 2008, **112**, 13488.
50. V. Biju, N. Sugathan, V. Vrinda and S. L. Salini, *Journal of Materials Science*, 2008, **43**, 1175.
51. W. Qin and J. A. Szpunar, *Philosophical Magazine Letters*, 2005, **85**, 649.
52. A. A. Nazarov, A. E. Romanov and R. Z. Valiev, *Nanostructured Materials*, 1994, **4**, 93.
53. Y. Kotolevich, E. Kolobova, E. Khramov, J. Cabrera Ortega, M. Farías, Y. Zubavichus and V. Cortés Corberán, *Molecules*, 2016, **21**, 532.
54. T. Tabakova, G. Avgouropoulos, J. Papavasiliou, M. Manzoli, F. Boccuzzi, K. Tenchev and T. Ioannides, *Applied Catalysis B: Environmental*, 2011, **101**, 256.
55. F. Arena, P. Famulari, G. Trunfio, G. Bonura, F. Frusteri and L. Spadaro, *Applied Catalysis B: Environmental*, 2006, **66**, 81.
56. G. Avgouropoulos, M. Manzoli, F. Boccuzzi, T. Tabakova, J. Papavasiliou, T. Ioannides and V. Idakiev, *Journal of Catalysis*, 2008, **256**, 237.
57. P. Kaminski, M. Ziolek, *Applied Catalysis B: Environmental*, 2016, **187**, 328.
58. A. Simakov, N. Bogdanchikova, I. Tuzovskaya, E. Smoletseva, A. Pestryakov, M. Farias, M. Avalos M.W. McCall, G. Dewar, M.A. Noginov, Complex Mediums VI: Light and Complexity, 2005, 5924, 101.
59. I. V. Tuzovskaya, A. V. Simakov, A. N. Pestryakov, N. E. Bogdanchikova, V. V. Gurin, M. H. Farías and M. Avalos, *Catalysis Communications*, 2007, **8**, 977.
60. E. Smolentseva, N. Bogdanchikova, A. Simakov, A. Pestryakov, M. Avalos, M.H.Farias, A. Tompos, V. Gurin, *Journal of Nanoscience and Nanotechnology*, 2007, **7**, 1882.
61. A. Pestryakov, V. Lunin, A. Kharlanov, D. Kochubey, N. Bogdanchikova and A. Y. Stakheev, *Journal of Molecular Structure*, 2002, **642**, 129.
62. A. N. Pestryakov, V. V. Lunin, A. N. Kharlanov, N. E. Bogdanchikova and I. V. Tuzovskaya, *The European Physical Journal D - Atomic, Molecular and Optical Physics*, 2003, **24**, 307.
63. E. Smolentseva, N. Bogdanchikova, A. Simakov, A. Pestryakov, I. Tusovskaya, M. Avalos and V. Gurin, *Surface Science*, 2006, **600**, 4256.

64. A. Pestryakov, I. Tuzovzkaya, E. Smolentseva, N. Bogdanchikova, F. C. Jentoft and A. Knop-Gericke, *International Journal of Modern Physics B*, 2005, **19**, 2321.
65. D.L. Feldheim, C.A. Foss, Metal Nanoparticles: Synthesis, Characterization and Applications, *Basel Marcel Dekker Inc.*, New York, 2002. 338 pp.
66. V. V. Costa, M. Estrada, Y. Demidova, I. Prosvirin, V. Kriventsov, R. F. Cotta and E. V. Gusevskaya, *Journal of Catalysis*, 2012, **292**, 148.
67. R. Feng, M. Li and J. Liu, *Colloids and Surfaces A: Physicochemical and Engineering Aspects*, 2012, **406**, 6.
68. C. Guzmán, G. del Ángel, R. Gómez, F. Galindo-Hernández and C. Ángeles-Chavez, *Catalysis Today*, 2011, **166**, 146.
69. F. Galindo-Hernández, J. A. Wang, R. Gómez, X. Bokhimi, L. Lartundo and A. Mantilla, *Journal of Photochemistry and Photobiology A: Chemistry*, 2012, **243**, 23.
70. A. Penkova, K. Chakarova, O. H. Laguna, K. Hadjiivanov, F. R. Saria, M. A. Centeno and J. A. Odriozola, *Catalysis Communications*, 2009, **10**, 1196.
71. B. Pawelec, P. Castaño and T. A. Zepeda, *Applied Surface Science*, 2008, **254**, 4092.
72. S. Peters, S. Peredkov, M. Neeb, W. Eberhardt and M. Al-Hada, *Surface Science*, 2013, **608**, 129.
73. J. Llorca, M. Domínguez, C. Ledesma, R. J. Chimentão, F. Medina, J. Sueiras and O. Rossell, *Journal of Catalysis*, 2008, **258**, 187.
74. G. M. Veith, A. R. Lupini, S. J. Pennycook, G. W. Ownby and N. J. Dudney, *Journal of Catalysis*, 2005, **231**, 151.
75. I. Tuzovskaya, N. Bogdanchikova, A. Simakov, V. Gurin, A. Pestryakov, M. Avalos and M. H. Farías, *Chemical Physics*, 2007, **338**, 23.
76. C.D. Wagner, M. Riggs, E. Davis, G. Müllenberg Handbook of X-ray Photoelectron spectroscopy, Perkin-Elmer Corp. Physical Electronics Division, Eden Prairie, MN, USA, 1979, 190 pp.
77. N. M. Figueiredo, N. J. M. Carvalho and A. Cavaleiro, *Applied Surface Science*, 2011, **257**, 5793.
78. P. H. Citrin, G. K. Wertheim and Y. Baer, *Physical Review B*, 1983, **27**, 3160.
79. M. P. Casaletto, A. Longo, A. Martorana, A. Prestianni and A. M. Venezia, *Surface and Interface Analysis*, 2006, **38**, 215.
80. A. Zwijnenburg, A. Goossens, W. G. Sloof, M. W. J. Crajé, A. M. van der Kraan, L. Jos de Jongh and J. A. Moulijn, *The Journal of Physical Chemistry B*, 2002, **106**, 9853.
81. S. Zafeiratos and S. Kennou, *Surface Science*, 1999, **443**, 238.
82. G. M. Veith, A. R. Lupini, S. J. Pennycook, G. W. Ownby and N. J. Dudney, *Journal of Catalysis*, 2005, **231**, 151.
83. T. Ishizaka, S. Muto and Y. Kurokawa, *Optics Communications*, 2001 **190**, 385.
84. O. Böse, E. Kemnitz, A. Lippitz, W. E. S. Unger and W. E. S. Unger, *Fresenius' Journal of Analytical Chemistry*, 1997, **358**, 175.
85. H. Piao and N. S. McIntyre, *Surface and Interface Analysis*, 2001, **31**, 874.
86. J. Radnik, C. Mohr, P. Claus, M. Haruta, C. Mohr, H. Hofmeister and B. Legrand, *Physical Chemistry Chemical Physics*, 2003, **5**, 172.
87. XPS Handbook of The Elements and Native Oxides *XPS International*, Inc. by Dr. B. Vincent Crist 1999, **1**, 87 p.
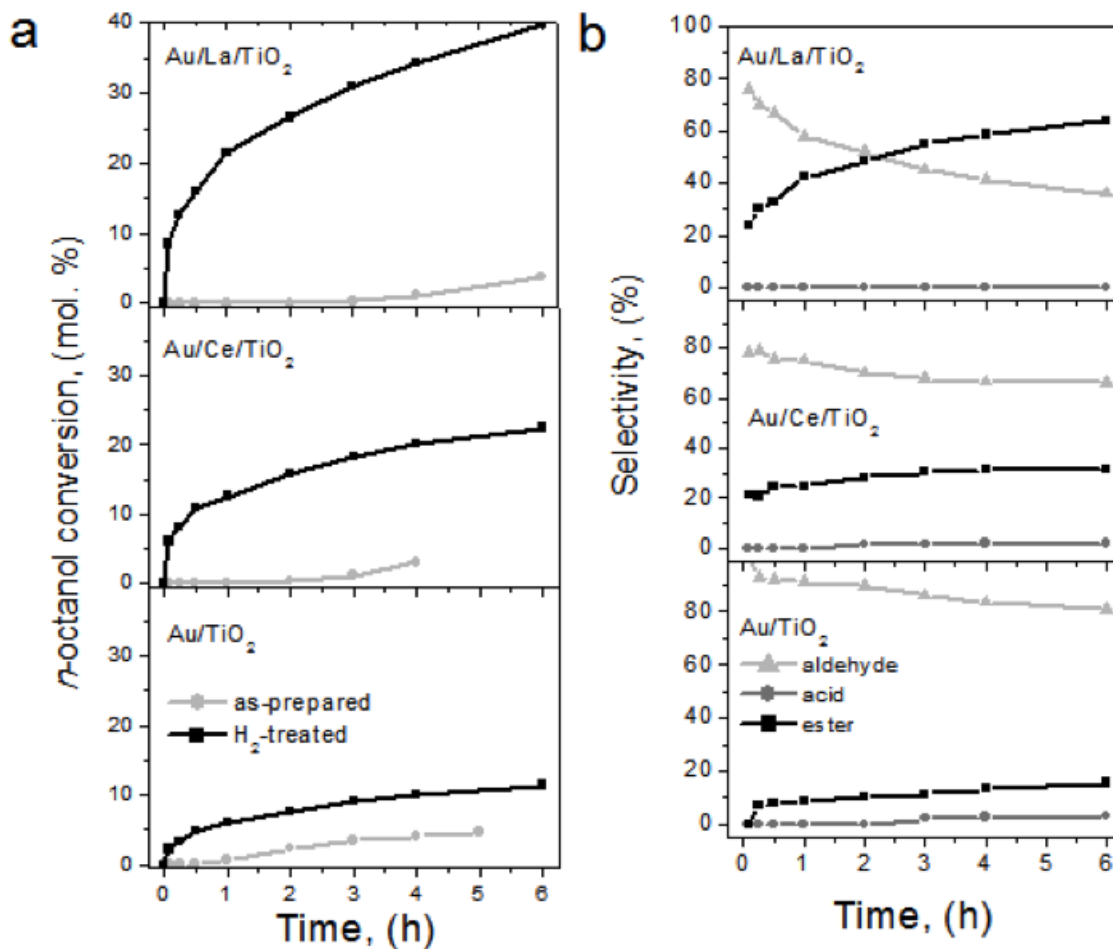
Fig. 1. Oxidation of 1-octanol on Au/TiO_2, $Au/La/TiO_2$ and $Au/Ce/TiO_2$ before and after treatment in H_2 flow (300°C, 1 h): (a) conversion *vs.* run time for as-prepared and H_2-treated catalysts and (b) products selectivity evolution with run time on catalysts after H_2 treatment.
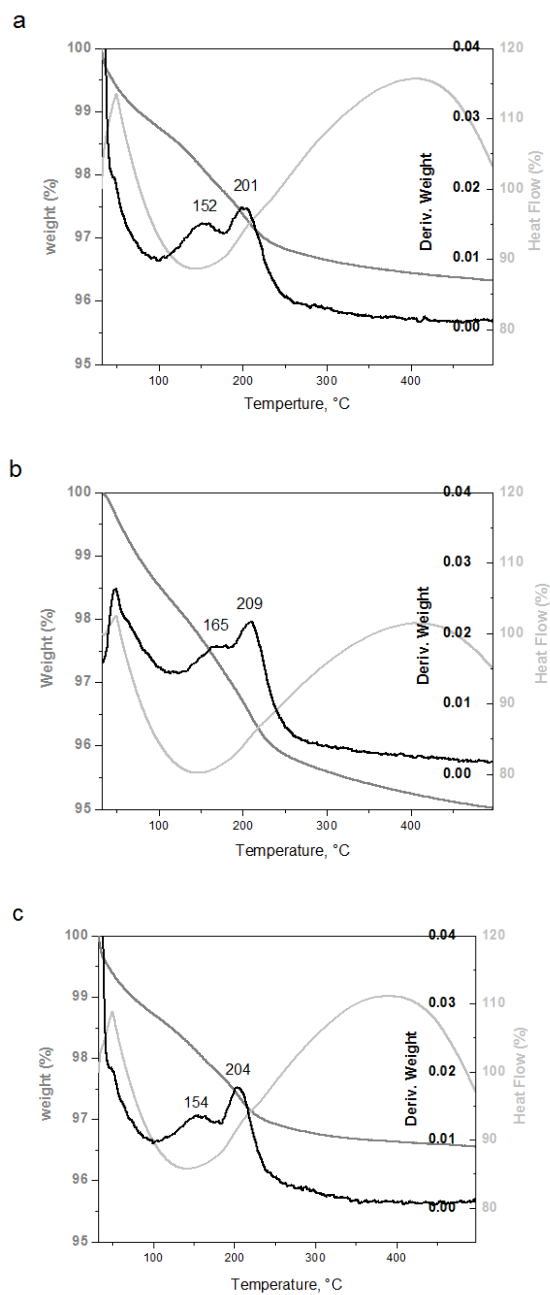
Fig. 2. TGA/DTA results in nitrogen flow (100 mL/min) for Au/TiO_2 (a), $Au/La/TiO_2$ (b) and $Au/Ce/TiO_2$ (c). Heating rate was 5°C/min.
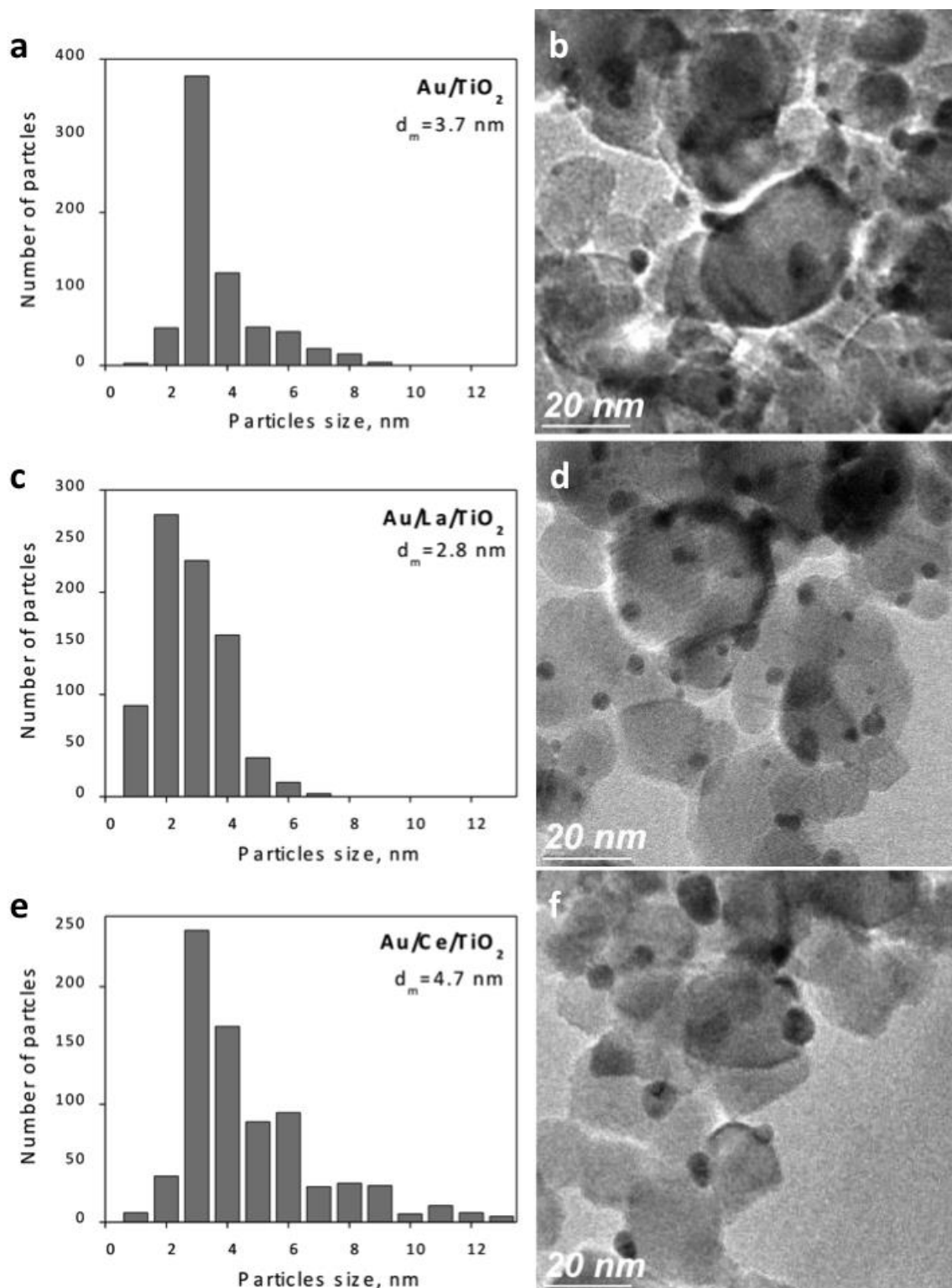
Fig. 3.   TEM Au particle size distribution and representative micrographs of catalysts Au/TiO_2 (b), $Au/La/TiO_2$ (d), and $Au/Ce/TiO_2$ (f) treated in H_2 flow at 300°C for 1 h.
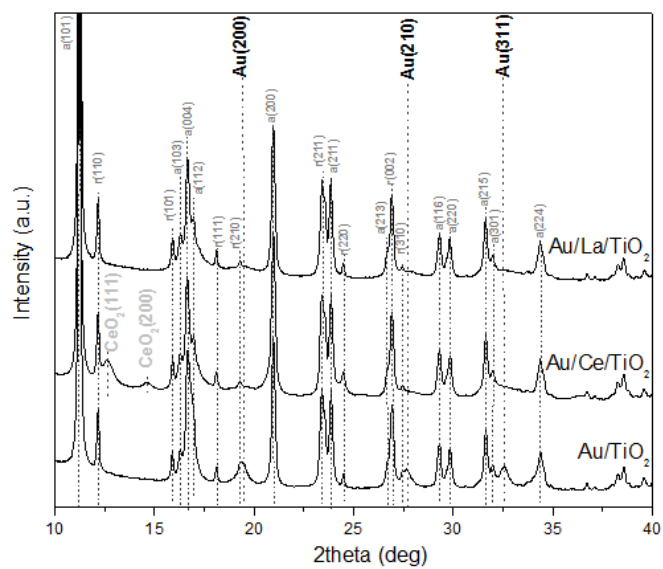
Fig. 4. SR-XRD patterns for catalysts treated in H_2 flow at 300°C for 1 h and their corresponding supports.
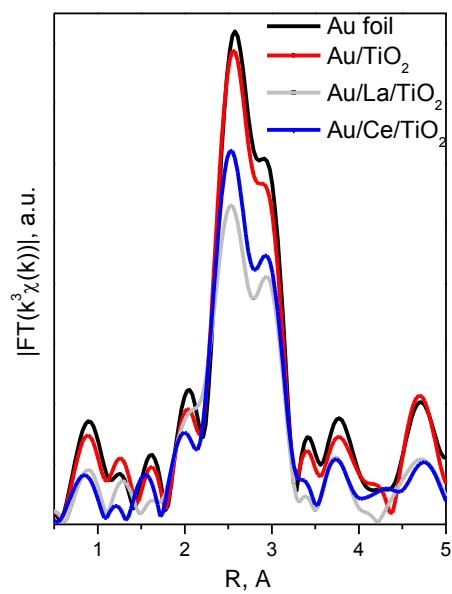
Fig. 5. Au L_3-edge EXAFS Fourier transforms for the catalysts after pretreatment in H_2 flow at 300ºC for 1 h.
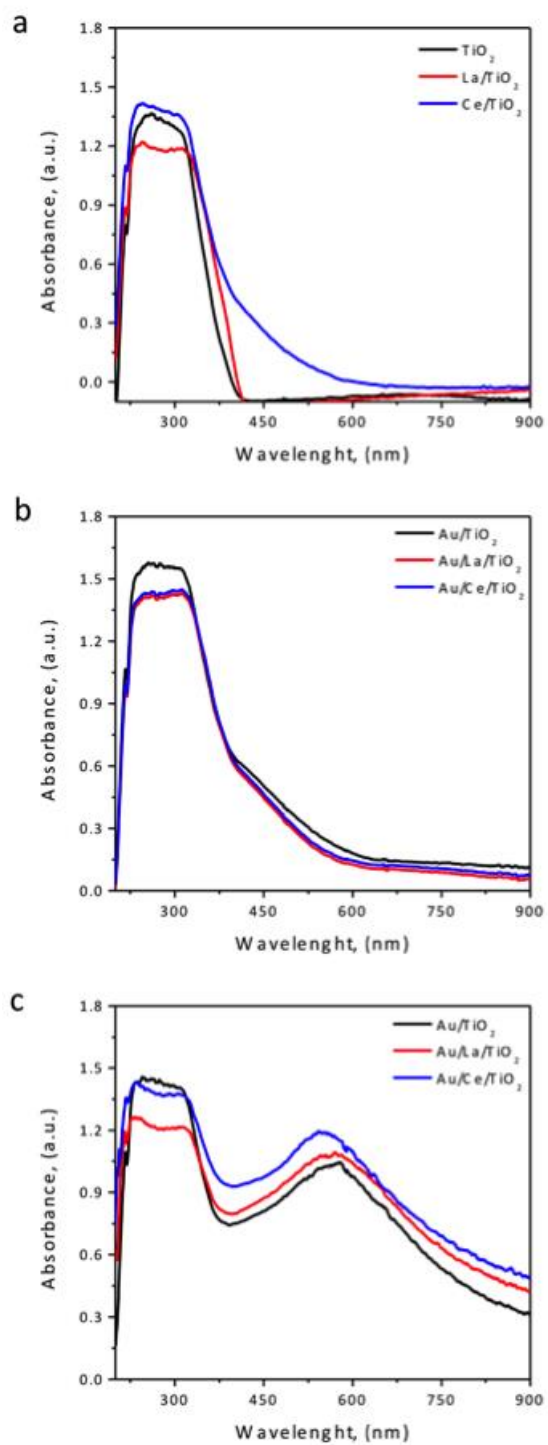
Fig. 6. DRS of supports (a) and catalysts, as-prepared (b) and pretreated in H_2 (300°C, 1 h) (c)
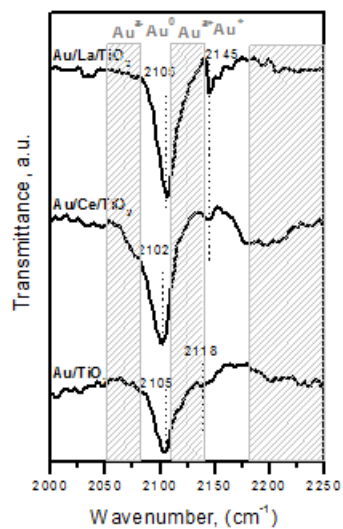
Fig. 7. FTIR spectra of CO adsorbed on the studied Au catalysts pretreated in H_2 or O_2 at 300°C for 1 h.
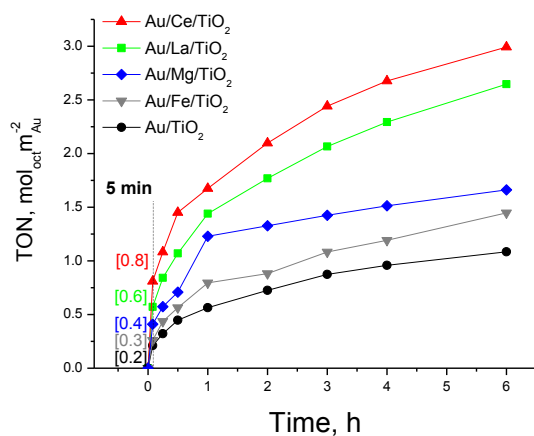
Fig. 8. Variation of TON for *n*-octanol oxidation on gold catalysts with run time. Numbers in square brackets indicate the respective TON after 5 min of reaction. Data for Au/Mg/TiO$_2$ and Au/Fe/TiO$_2$ are from our recent publication [23].
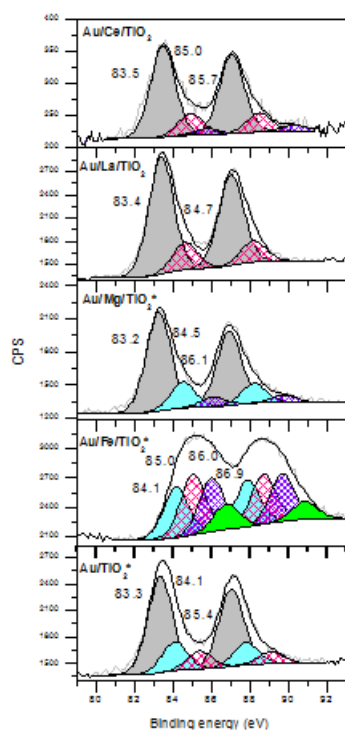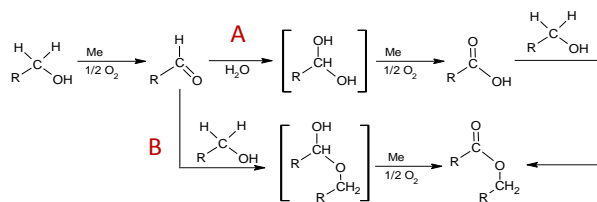
Fig. 9. XPS 4f photoelectron spectra of Au NPs of gold catalysts supported on bare or modified titania after reduction in H_2 under 300°C for 1 h. (*) Data for Au/Mg/TiO$_2$ and Au/Fe/TiO$_2$ are from our recent publication [23].

Scheme 1. Plausible reaction pathways for the oxidation of 1-octanol over supported gold catalysts

Table 1. Gold content and specific surface area of supports and catalysts treated in H_2 flow at 300ºC for 1 h.

Samples	S_{BET}, m^2/g		Au content, wt. %
	Support	Catalyst	
Au/TiO$_2$	55.5	45.5	4.5±0.4
Au/La/TiO$_2$	45.3	45.2	3.6±0.3
Au/Ce/TiO$_2$	43.4	46.6	3.5±0.3

Table 2. Au NPs structural parameters obtained from Rietveld refinement of SR-XRD patterns and EXAFS Fourier transform fitting for catalysts treated in H_2 flow at 300°C for 1 h.

Sample	SR-XRD		EXAFS	
	Lattice constant, Å	Scherrer size, nm	Coordination number	Interatomic distance, Å
Au/TiO$_2$	4.0771	17.7	11.9	2.873
Au/La/TiO$_2$	4.0669	5.1	9.8	2.855
Au/Ce/TiO$_2$	4.0733	4.7	11.1	2.858
Au foil	-		12.0	2.888

Table 3. XPS binding energy and relative atomic concentration (in %) of the different gold stages in the studied catalysts after reduction in H_2 at 300°C for 1 h.

Catalysts	BE of different gold electronic states (eV), and their relative atomic concretions, % (indicated in parenthesis)					Ref.
	$Au_n^{\delta-}$	Au^0	Au^+	Au_2O_x (1<x<3)	Au^{3+}	
	≤ 83.6 [†]	**~84.0** [†]	**~85.0** [†]	**~86.0** [†]	**~87.0** [†]	
Au/Ce/TiO$_2$	83.5 (76%)	-	85.0 (18%)	85.7 (6%)	-	Present work
Au/La/TiO$_2$	83.4 (81%)	-	84.7 (19%)	-	-	
Au/Mg/TiO$_2$	83.2 (73%)	84.5 (20%)	-	86.1 (7%)	-	[23]
Au/Fe/TiO$_2$	-	84.1 (28%)	85.0 (32%)	86.0 (29%)	86.9 (11%)	
Au/TiO$_2$	83.3 (68%)	84.1 (20%)	85.4 (12%)	-	-	

† Bold numbers refer to BE data from literature [62-77]